◆ Human Brain Mapping 39:354–368 (2018) ◆

Functional Subdivisions Within the Human Intraparietal Sulcus are Involved in Visuospatial Transformation in a Non-Context-Dependent Manner

Alexandra Papadopoulos,[1,2] Francesco Sforazzini,[2] Gary Egan,[1,2,3] and Sharna Jamadar [1,2,3]*

[1]*Monash Institute of Cognitive and Clinical Neuroscience, School of Psychological Sciences, Monash University, Melbourne, Victoria 3800, Australia*
[2]*Monash Biomedical Imaging, Monash University, Melbourne, Victoria 3800, Australia*
[3]*Australian Research Council Centre of Excellence for Integrative Brain Function, Australia*

Abstract: Object-based visuospatial transformation is important for the ability to interact with the world and the people and objects within it. In this preliminary investigation, we hypothesized that object-based visuospatial transformation is a unitary process invoked regardless of current context and is localized to the intraparietal sulcus. Participants ($n = 14$) performed both antisaccade and mental rotation tasks while scanned using fMRI. A statistical conjunction confirmed that both tasks activated the intraparietal sulcus. Statistical parametric anatomical mapping determined that the statistical conjunction was localized to intraparietal sulcus subregions hIP2 and hIP3. A Gaussian naïve Bayes classifier confirmed that the conjunction in region hIP3 was indistinguishable between tasks. The results provide evidence that object-based visuospatial transformation is a domain-general process that is invoked regardless of current context. Our results are consistent with the modular model of the posterior parietal cortex and the distinct cytoarchitectonic, structural, and functional connectivity profiles of the subregions in the intraparietal sulcus. *Hum Brain Mapp 39:354–368, 2018.*

Key words: intraparietal sulcus; visuospatial transformation; antisaccade; mental rotation; fMRI

INTRODUCTION

The intraparietal sulcus (IPS) plays a fundamental role in organizing visual spatial attention. A wide range of processes activate the IPS, with neurons encoding information such as spatial coordinates of objects, the position of body parts in space, eye movement data, or geometrical properties of objects such as shape, size, and orientation [Grefkes and Fink, 2005]. A potential commonality between these processes is that all require some form of visuospatial transformation within an object-based reference frame, in contrast to other visuospatial transformations that are performed in the

Contract grant sponsor: Australian Research Council Discovery Early Career Researcher Award; Contract grant number: DE150100406; Contract grant sponsor: Australian Research Council Centre of Excellence for Integrative Brain Function; Contract grant number: CE140100007.

*Correspondence to: Sharna Jamadar; Monash Institute for Cognitive and Clinical Neuroscience, Monash Biomedical Imaging, 770 Blackburn Rd, Clayton, Victoria 3800, Australia.
E-mail: sharna.jamadar@monash.edu

Received for publication 16 August 2017; Revised 26 September 2017; Accepted 4 October 2017.

DOI: 10.1002/hbm.23847
Published online 23 October 2017 in Wiley Online Library (wileyonlinelibrary.com).

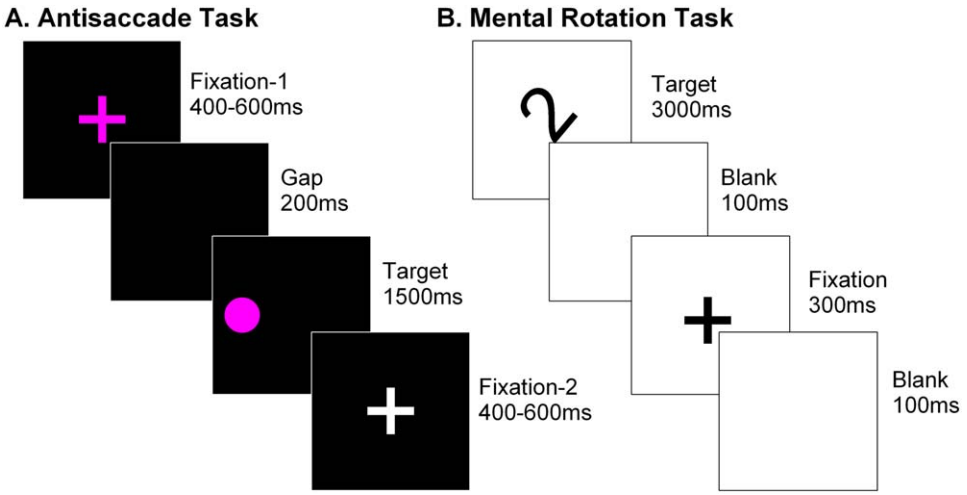

Figure 1.

Task design. (a) Antisaccade task. Figure represents a single trial. Depending on the color of fixation-1 and the target, the participant was required to make a prosaccade toward the target or an antisaccade to the mirror opposite location. Color-task mapping was randomized between participants. (b) Mental rotation task. Figure represents a single trial. [Color figure can be viewed at wileyonlinelibrary.com]

egocentric (relative to self or effector) and allocentric (relative to environmental fiducial points) reference frame (see Zacks and Michelon [2005] for a review). Despite highly consistent activation of the IPS in tasks requiring object-based visuospatial transformation, it remains unclear if the IPS plays a "general purpose" role in the transformation that is invoked regardless of current context (i.e., current behavioral goals).

Two tasks that show robust activation of the IPS are the mental rotation and antisaccade tasks. The mental rotation task requires the imagined rotation of a visual stimulus from one orientation to another, for example, the imagined rotation of a digit to determine if it is presented in its correct or reversed orientation [Podzebenko et al., 2002; Fig. 1B]. The antisaccade task requires an eye movement away from a peripherally presented target to its mirror opposite location (Fig. 1A); in other words, it requires the transformation of the target location to a mirror opposite location. Despite clear differences in task parameters including imagined versus overt movement, the category-response task rules, and stimulus visual and temporal characteristics, activations for both tasks have been identified within the IPS. Our aim was to investigate whether the IPS may have a general-purpose role in object-based spatial transformations that is activated regardless of the task context.

A vast number of studies have attempted to map the structure and function of the IPS. Much of the published research has exploited the apparent anatomical and functional similarities of the human and nonhuman primate IPS, leading to the identification of neurons that respond to direction in the visuomotor domain [Grefkes and Fink, 2005], including a "remapped vector signal" required in the antisaccade task [Zhang and Barash, 2000]. The nonhuman primate (NHP) IPS has been subdivided into a number of subregions, including the anterior intraparietal area (AIP) which selectively activates for size, shape, and orientation of objects, especially where the objects are targets for motor manipulation; the medial intraparietal area (MIP) which is involved in planning, executing and monitoring reaching movements; the ventral intraparietal area (VIP) which is a "polymodal" association region, integrating visual, tactile, vestibular, and auditory input; the lateral intraparietal area (LIP) which is particularly responsive during saccades; and the caudal intraparietal area (CIP) which is particularly involved in the processing of 3D object features.

The human parietal cortex is greatly expanded in comparison to nonhuman primates [Grefkes and Fink, 2005; see also Mitchell et al., 2016], which results in different spatial positions of distinct anatomical IPS subregions, as well as the presence of anatomical and functional areas unique to humans. Cytoarchitectonic studies have identified three distinct IPS subdivisions: hIP1, hIP2, and hIP3 [Choi et al., 2006; Scheperjans et al., 2008a, 2008b]. These regions are postulated to be putative homologs of macaque AIP, VIP, and MIP respectively [Caspers et al., 2012]. The IPS anatomical subdivisions exhibit quite different functional activity and connectivity to different neural networks [Uddin et al., 2010]. Functional connectivity analyses have shown that hIP1 and hIP2 (located anteriorly on the IPS) have a strong association with frontal attentional regions, while hIP3 (located more posteriorly) shows strong coupling with posterior occipital regions.

A saccade is a fast eye movement that quickly moves the fovea from one target or image to another [Enderle,

2010]. The antisaccade task requires participants to inhibit a reflexive saccade to a visual target and instead make a voluntary saccade to its mirror opposite location [Munoz and Everling, 2004]. Neuroimaging and single cell recording studies of NHPs and humans have revealed that the IPS and the posterior superior parietal lobule play a major role in generating saccades [Koyama et al., 2004; McDowell et al., 2008; Sereno et al., 2001; Zhang and Barash, 2000]. A recent meta-analysis of neuroimaging studies of the antisaccade task in humans confirmed that the IPS is highly activated while performing antisaccades compared to prosaccades [Jamadar et al., 2013]. In the antisaccade task, the IPS is thought to be involved in the process of vector inversion [Brown et al., 2006; Medendorp et al., 2005] that spatially transforms the target for the saccade from the visually presented stimulus location to the mirror opposite location [Domagalik et al., 2012; Dyckman et al., 2007; Moon et al., 2007; Nyffeler et al., 2007]. Single-cell recordings in NHPs have shown that the vector inversion process is localized to the NHP lateral intraparietal region [Zhang and Barash, 2000]. The human equivalent of NHP lateral intraparietal area is thought to be on the posterior medial wall of the IPS [Culham and Valyear, 2006; McDowell et al., 2008; Pierrot-Deseilligny et al., 2009].

During the mental rotation task, subjects are required to imagine rotating a visually presented stimulus from one orientation to another. Reaction time increases with increasing angle of imagined rotation [Alivisatos and Petrides, 1997; Cohen et al., 1996; Goebel et al., 1998; Gogos et al., 2010; Schendan and Stern, 2007; Zacks, 2008]. The superior parietal lobule has a significant role in the mental rotation process with activation identified along with the IPS [Booth et al., 2000; Gogos et al., 2010; Zacks, 2008]. Additionally, specific subregions of the IPS are selectively activated during mental rotation, namely, the ventrolateral bank of the IPS [Podzebenko et al., 2005], the ventral and dorsal IPS [Milivojevic et al., 2009; Schendan and Stern, 2007], and the medial and posterior medial IPS [Weiss et al., 2009]. The medial and posterior medial aspects of the IPS are frequently involved in mental rotation and antisaccade tasks.

Both mental rotation and antisaccade tasks require object-based visuospatial transformation, and both reliably and robustly activate the IPS. Therefore, we aimed to determine whether the IPS may have a general-purpose role in object-based visuospatial transformation that is invoked regardless of the current task context. We conjectured that the IPS may play a unitary role in object-based visuospatial transformation. In this initial study, we conducted functional MRI in a cohort of young healthy individuals while they completed mental rotation and antisaccade tasks. We conducted a statistical conjunction analysis to determine whether both tasks activated the same IPS regions. A consistency analysis was conducted to identify how consistent IPS activity was across the participants, and a classifier analysis was performed to determine if activity between the two tasks within the IPS region was statistically distinguishable. We hypothesized that the medial and the posterior IPS would be active during antisaccades, and that the ventrolateral bank of the IPS, ventral, posterior medial, and medial IPS would be active during mental rotation. Finally, we also hypothesized that both tasks would activate overlapping regions in the IPS, specifically, the medial IPS region and the posterior medial IPS region corresponding to cytoarchitectonic region hIP3.

METHODS

All procedures were reviewed and approved by the Monash University Human Research Ethics Committee, in accordance with the Australian National Statement on Ethical Conduct in Human Research (2007).

Participants

Nineteen healthy participants volunteered in this study. Two participants had incomplete behavioral data sets and one participant experienced difficulty remaining in the MRI scanner due to claustrophobia; therefore, the data for these three participants were excluded from the overall analysis. Additionally, two participants were excluded due to poor performance on either task (<50% correct). The remaining 14 participants (aged 23–42 years, mean 29.1, SD = 5.85 years, 6 female) were predominantly right handed (9 right, 3 left, 2 ambidextrous; Edinburgh Handedness Inventory, Oldfield, [1971]) with mean 19.8 (SD 3.2) years of education. All participants had normal or corrected-to-normal vision, had no history of neurological impairment or head trauma; women were excluded for current or suspected pregnancy.

Stimuli and Tasks

Stimuli for each task were projected onto a 1.2 m × 1 m screen positioned at the rear of the MRI scanner bore. While in the scanner, participants lay supine with their head supported in a 20-channel radiofrequency head coil, with foam padding used to reduce motion. Participants viewed the screen with an angled mirror attached to the head coil. Earplugs were used to reduce the discomfort of scanner noise.

Antisaccade task

The antisaccade task was programmed in Experiment Builder v.10 (SR Research, Ontario Canada). Antisaccade, prosaccade, and null trials were presented using a block design in pseudorandomized order (e.g., AS/null/PS/null/PS/null/AS/null…). There were nine cycles of antisaccade/null/prosaccade/null sequence. Participants completed 99 trials each of antisaccade and prosaccade.

The duration of antisaccade and prosaccade trials were fixed at 2700 ms. Each trial began with the presentation of a fixation cross ("fixation-1" 96 × 96 pixels; Fig. 1A) on a black background presented for 400, 450, 500, 550, or 600 ms with the duration randomized between trials. The fixation-1 image was removed and followed by a blank screen (200 ms), after which the target (filled circle diameter 96 pixels with 30 × 30 pixel cross hairs in center) appeared on either the left or the right side of the screen for 1500 ms. The target was followed by a white fixation cross ("fixation-2," 96 × 96 pixels) until the end of the trial for 600, 550, 500, 450, or 400 ms, randomized between trials. One block of each task type consisted of 11 trials with a duration of 29.7 s.

For the antisaccade and prosaccade trials, the fixation-1 image and the target were colored in one of two cue colors; magenta for antisaccade, turquoise for prosaccade or vice versa, counterbalanced between participants. Within antisaccade and prosaccade blocks, trials were pseudorandomized according to the following rules: even number of right and left targets within trial type, no more than four consecutive targets in the same hemisphere, the fixation cross duration randomized with equal number of each within trial type, and no more than four consecutive trials of the same fixation cross duration. Participants were instructed to direct their gaze to the fixation cross and when the colored target appeared, to execute an eye movement either to the stimulus (prosaccade) or to its mirror opposite location (antisaccade) indicated by the target color. The fixation-2 image then appeared to indicate the end of that trial type and the start of the next trial. For null trials, the fixation-1 image was white and was presented continuously on the screen for 16.2 s. Six trials made up one null block. Participants were instructed to maintain fixation throughout the duration of the null block. Total task run time was 13.8 min.

Mental rotation task

Stimuli were presented using Presentation software (v12, Neurobehavioral Systems, CA, USA). The mental rotation task was based on a previous study [Gogos et al., 2010] and consisted of six two-dimensional alphanumeric characters (F, G, R, 2, 4, 5) presented in their normal or mirror-reverse orientation (Fig. 1B). The characters were displayed in their upright position or at varying angles of rotation, ranging from 0° to 320°. There were seven available rotation angles that were divided into four groups of average rotation angle; (i) stimuli not rotated (0°, zero), (ii) 50° average rotation (included stimuli rotated 40/320° and 60/300°), (iii) 100° average rotation (included stimuli rotated 80/280°, 100/260°, and 120/240°), and (iv) 150° average rotation (included stimuli rotated 140/220° and 160/200°). Thus the five experimental conditions were a baseline, a 0° rotation condition and three rotation conditions; easy (50° average rotation), medium (100° average rotation), and hard (150° average rotation).

The five conditions were presented in a block design over two runs (8 min 24 s each; 288 total trials). A total of 24 blocks were presented pseudorandomly per run: six baseline, six 0° rotation and four 50°, four 100°, and four 150° rotation blocks. Each block lasted 21 s and consisted of six trials of 3500 ms per trial. Each stimulus was presented in black Arial font in the center of a white screen for 3000 ms, followed by a blank white screen for 100 ms, fixation point ("+") for 300 ms and another blank white screen for 100 ms. The first and last block in each run was a baseline condition. In the baseline condition, six consecutive presentations of an arrow pointing to the left or right required participants to respond with the hand corresponding with the arrow direction. For rotated stimuli, participants were asked to determine stimulus orientation and responded by pressing a button corresponding to "correct" orientation or "mirror-reverse" orientation. Participants held a response pad in each hand and responded with the index finger of each hand; right hand to indicate correct and left hand to indicate mirror reverse orientation or vice versa, counterbalanced between participants.

In each run, there were a total of 108 alphanumeric stimuli, consisting of 18 trials of each of the six characters. The sequence of stimuli within each run was consistent between all participants; however, the order in which the runs were presented differed between participants.

Data Acquisition and Analysis

Antisaccade task: Ocular motor data recording and analysis

Horizontal displacement of the eye was recorded simultaneously with fMRI using an MR- compatible video-based SR Research Eyelink 1000 system, with a spatial resolution of 0.01° and a sampling rate of 500 Hz.

Ocular motor data were analyzed using a customized program written in MatLab (v.8.0, R2012b) and was used to mark the time and location of target onset and offset, as well as saccade onset and offset. Each trial was manually inspected to ensure correct placement of target and saccade markers and to ascertain errors. The onset of the saccade was defined as the time when eye velocity exceeded 30°/s and the end of a saccade was defined as the time after saccade onset when eye velocity fell below 10°/s. Trials were excluded from further behavioral analysis if they exhibited: (i) blinks prior to 100 ms of the target onset or during the primary saccade, (ii) small saccades with amplitude $< 3°$, or (iii) anticipatory eye movements (saccades made within 100 ms of the peripheral target appearing). On average, 37 trials were excluded from the behavioral analysis using these criteria. Variables of interest were reaction time of the primary saccade (the time difference between target onset and the primary saccade onset) and directional errors (trials in which a prosaccade was made during an antisaccade trial, or in which an antisaccade was made during a prosaccade trial). Directional error proportions were calculated for both

pro- and antisaccades as the ratio of the number of trials with a directional error to the total number of trials analyzed. Outliers (values exceeding ± 3 SDs) for these variables were removed.

Behavioral data were analyzed using IBM SPSS Statistics 20. Reaction time and directional error percentage were analyzed with two separate 2 trial type (antisaccade and prosaccade) repeated measures ANOVA. Estimates of effect size are partial eta squared.

Mental rotation task: Behavioral data recording and analysis

Reaction time and percentage correct were the variables of interest. Behavioral data were analyzed using IBM SPSS Statistics 20. Reaction time and percentage correct were analyzed with two separate 3 trial type (easy, medium, and hard) repeated measures ANOVA. Estimates of effect size are partial eta squared.

Behavioral results were not corrected for multiple comparisons for the number of tasks (antisaccade and mental rotation) or the number of measures for each task (RT and error rate).

MR image acquisition and analysis

Magnetic resonance images were acquired on a Siemens Skyra 3 T wide-bore scanner equipped with a Siemens 20 channel radiofrequency head coil. Functional MRI was acquired using a T2*-weighted GRAPPA echo-planar imaging (EPI) sequence (ascending axial acquisition, TR = 2.5 s, TE = 30 ms, FOV = 192 mm, acquisition matrix = 64 × 64, 44 slices, 3 × 3 × 3 mm voxels). Structural MRI was acquired using a T1-weighted 3D MPRAGE sequence (TR = 1900 ms, TE = 2.43 ms, flip angle = 9°, matrix = 192 × 192 mm, voxel size = 0.6 × 0.6 × 0.6 mm^3, 256 slices). For the antisaccade task, a total of 356 volumes were acquired per run, while for the mental rotation task, a total of 211 volumes were acquired per run.

MRI data were analyzed with Statistical Parametric Mapping 8 (SPM8; Wellcome Department of Cognitive Neurology, London). Data from both tasks for each participant were preprocessed and modeled separately. For functional runs, the first five images of each participant for each task were discarded to account for T1 saturation effects. EPI slice acquisition timing differences were corrected using the central slice as a reference, realigned to the first nondummy image and coregistered to their individual structural scans. Structural scans were then segmented using the unified segmentation algorithm in SPM8 to derive spatial normalization parameters for each individual to MNI space. Functional and structural scans were then normalized to the MNI template using these parameters and spatially smoothed using a 3 mm isotropic full width half maximum (FWHM) Gaussian smoothing kernel. A small smoothing kernel was chosen to reduce the blurring of effects across the IPS subregions. Mean total displacement [Wilke, 2012, 2014] across subjects was 0.64 mm (s.d. 0.32 mm; range 0.38–1.17 mm). No participant met criteria for exclusion for motion (acute motion >1 voxel).

For the antisaccade task, first-level analyses consisted of a model with the two experimental regressors (antisaccade and prosaccade) and six realignment parameters (x, y, z, pitch, roll and yaw) as regressors of no interest, convolved with a canonical hemodynamic response. Contrast images for antisaccade compared to baseline were entered into a second-level random effects analysis and thresholded ($P_{\text{FDR corrected}} < 0.05$, $k > 25$ voxels).

For the mental rotation task, first-level analyses consisted of a model with the four experimental regressors (zero, easy, medium, and hard) and six realignment parameters (x, y, z, pitch, roll, and yaw) convolved with a canonical hemodynamic response. Contrast images for hard > zero were entered into a second-level random effects analysis and thresholded ($P_{\text{FDR corrected}} < 0.05$, $k > 25$ voxels). The hard > zero contrast was used to identify the maximal mental rotation activation in the IPS.

IPS ROI definition and conjunction analyses

Anatomical regions of interest (ROI) were defined using maximum probability cytoarchitectonic maps in the SPM Anatomy toolbox [Eickhoff et al., 2005]. The probabilistic cytoarchitectonic maps are based on an observer-independent cytoarchitectonic analysis in a sample of 10 human postmortem brains, and provide stereotaxic information on the location and variability of cortical areas in the Montreal Neurological Institute (MNI) reference space [Eickhoff et al., 2006]. Details on the IPS cytoarchitectonic regions that these maps are based on are found in Caspers et al. [2008, 2012], Choi et al. [2006], Hoffstaedter et al. [2013], Scheperjans et al. [2008a, 2008b], and Wu et al. [2009]. The combined IPS map used in this analysis included the human intraparietal areas 1, 2, and 3 (hIP1, hIP2, and hIP3, respectively). The probability threshold was set to $P < 0.05$ and the number of voxels contained in regions hIP1, 2, and 3 at this threshold were 5433 (1173 mm^3), 2802 (605 mm^3), and 4620 (997 mm^3), respectively. Separate conjunction analyses of each task with the combined IPS map were performed. A task conjunction map of co-activation within the IPS during both the antisaccade and mental rotation tasks was computed, and conjunction analyses were performed between the individual hIP maps, areas BA2 and SPL7PC, with the task conjunction map.

Consistency analysis and nonparametric tests

To determine the consistency of the results across subjects, we calculated the number of participants contributing to each cluster. Each participant's first-level antisaccade and mental rotation thresholded maps were binarized to produce maps with values of 0 (no activity) or 1 (activity). A group-level consistency map was calculated to quantify the number of participants with activity in each cluster.

In addition to this consistency analysis, we also conducted nonparametric tests to examine the reproducibility of the conjunction analysis, controlling for sample variance in age, sex, and handedness. Permutation analysis was performed using FSL Randomize. Specifically, Z-maps for all the 14 subjects for each task were merged to create 2 4D files. Each of them was then fed into Randomize with 5000 permutations, controlling for age, gender, and handedness. Permutation tests were limited to the IPS region. The P values in the final images were FWE $P < 0.05$ corrected, controlling for false-positive rate. Finally, the conjunction map was calculated taking the maximum of the $1 - P$ values in each voxel between the two tasks.

Classifier analysis

While a statistically significant conjunction provides evidence of co-activation of the same region between tasks, this analysis does not provide information that the activity is identical between the two tasks. To do this, a classification algorithm is required.

The activation maps for each participant were divided into two classes (the antisaccade and mental rotation maps), with 14 exemplars per class, and a decoding analysis was performed using the IPS map as the ROI mask. The activation maps were converted to Z-score and submitted to a leave-one-run-out cross-validation scheme, using a Gaussian Naïve Bayes (GNB) classifier and a searchlight approach (searchlight radius of 4 voxels). Briefly, each voxel in the IPS mask was used as a center to build a searchlight sphere of radius 4 voxels (including only those voxels within the IPS map). This sphere was used to extract the voxel values for each participant's activation map, to create an $N \times M$ classifier matrix (where N is the total number of exemplars, 28, and M is the number of voxels within the sphere). An exemplar (per class) was left out, and a prediction for its label was made using the classifier trained on the remaining sample (26 exemplars). This procedure was repeated for each exemplar in turn to generate 28 predictions. The accuracy for the voxel in the center of the searchlight sphere was then computed as the proportion of the number of correct classifications to the total number of predictions. In this way, an accuracy value was produced for each voxel of the IPS mask. To assess statistical significance, a permutation test within each searchlight step (8192 permutations which is the maximum possible number for this analysis) was implemented (Hebart et al., 2015) and the accuracy map was thresholded at $P < 0.05$. To further investigate the classification accuracy, the decoding analysis was repeated using three independent ROIs, namely hIP1, hIP2, and hIP3, respectively.

Finally, the IPS subregion accuracy maps were binarized (1 in voxels with accuracy $> 50\%$, 0 otherwise) to determine the proportion of the subregion that was classified at $>50\%$ accuracy. The Dice Similarity Coefficient (DSC) was used to quantify the spatial overlap between the binarized accuracy maps and the three IPS subregion maps. The DSC is given by

$$\frac{2(X \cap Y)}{|X|+|Y|}$$

where the first term is the number of common voxels between the two masks, and $|X|$ and $|Y|$ are the total number of nonzero voxels in the first and second masks, respectively. The value of the Dice coefficient ranges from 0 (no spatial overlap between two binary images) to 1 for complete overlap. Three Dice scores were calculated for the accuracy maps for hIP1, hIP2, and hIP3.

RESULTS

Behavioral Results

Reaction times (Fig. 2A) were significantly longer for antisaccades compared to prosaccades ($F(1,13) = 102.809$, $P = 1.53 \times 10^{-7}$, $\eta^2 = 0.888$). Mean directional error rates (accuracy) showed antisaccades had higher rates compared to prosaccades but this was not significant ($F(1,13) = 3.866$, $P = 0.071$, $\eta^2 = 0.229$).

For the mental rotation task, reaction time (Fig. 2B) significantly increased as a function of increasing rotation angle (easy, medium and hard: $F(2,26) = 79.046$, $P = 8.90 \times 10^{-12}$, $\eta^2 = 0.859$). Accuracy (percent correct) reduced significantly (Fig. 2B) with increasing rotation angle ($F(2,26) = 18.083$, $P = 1.2 \times 10^{-5}$, $\eta^2 = 0.582$). The reduced accuracy with increasing rotation angle was significant for the easy versus hard conditions ($P = 1.4 \times 10^{-4}$), and for the medium versus hard conditions ($P = 0.001$), but no significant differences were observed for the easy versus medium conditions ($P = 0.137$; planned comparisons).

Functional MRI Results

Activation maps results for each task across the whole brain are shown in Figure 3. Consistent with previous studies, both the antisaccade task and mental rotation task evoked activation in distributed frontal-parietal networks. Results for the conjunction analysis across the whole brain are shown in Figure 3c. As expected following the individual task analyses, the task conjunction analysis identified activation in a distributed frontal-parietal network.

Results for the IPS activation for each task are shown in Figure 4. The antisaccade task evoked activation along the medial bank of the IPS (Fig. 4A) that extended from anterior to posterior IPS, predominantly within the right hemisphere. The mental rotation task showed similar activation to the antisaccade task within the IPS (Fig. 4B) with notable activation in the posterior medial IPS region. The task conjunction analysis showed significant co-localized activation for the two tasks within the IPS (Fig. 4C), extending

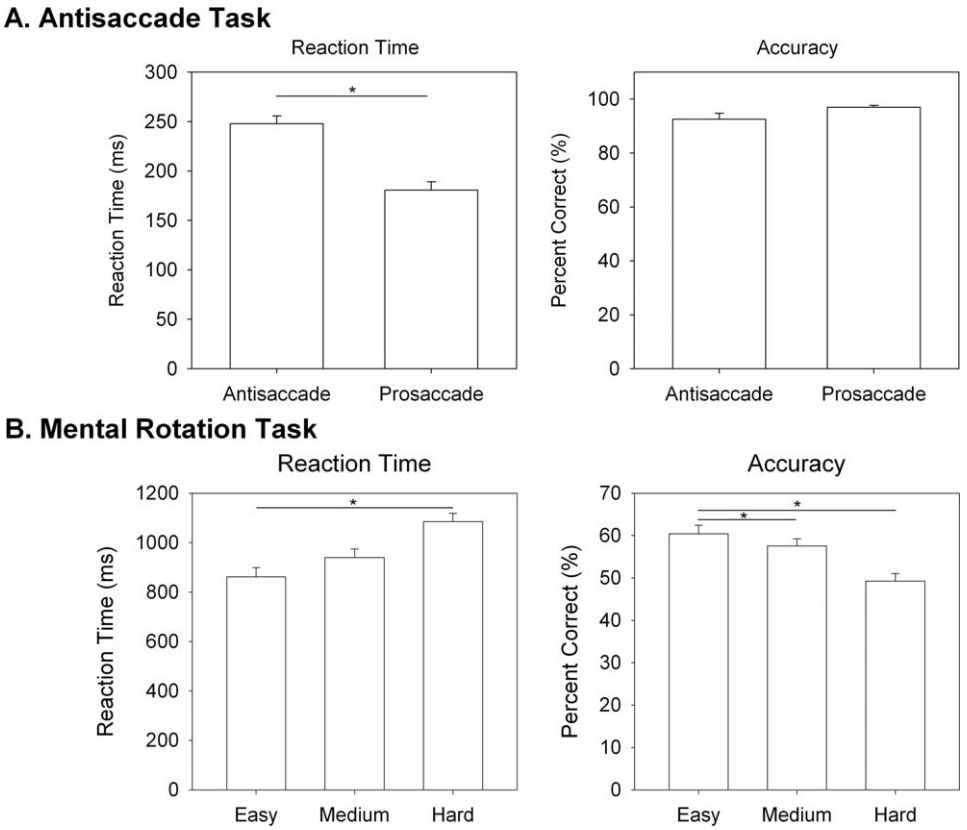

Figure 2.

Behavioral results. (a) Reaction time and accuracy for the antisaccade task. (b) Reaction time and error rate for the mental rotation task. Error bars show standard error. Horizontal bars and asterisks indicate significant effects of condition (see Behavioral Results).

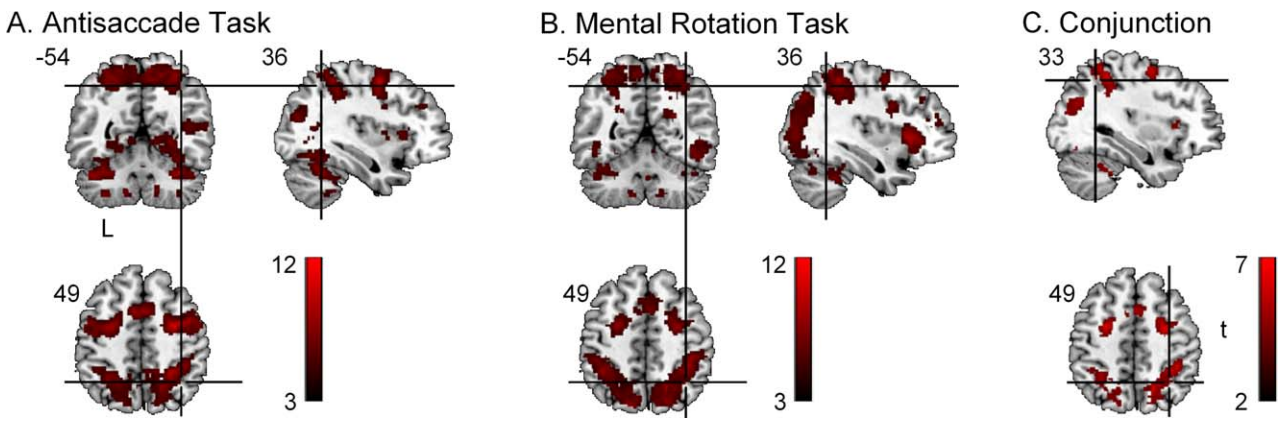

Figure 3.

Whole-brain activation results in the IPS. (a) Antisaccade activation map for the antisaccade > baseline contrast (Talairach coordinate $x = 36$, $y = -54$, $z = 49$); (b) mental rotation task for the hard > zero contrast (36, −54, 49); and (c) the task conjunction map between the antisaccade and mental rotation activation maps ($x = 33$, $z = 49$). [Color figure can be viewed at wileyonlinelibrary.com]

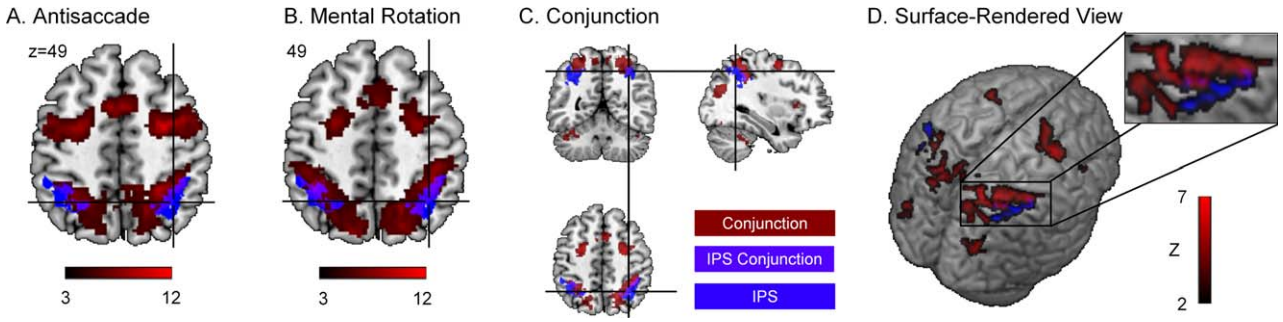

Figure 4.

IPS task conjunction maps. Overlap of the IPS mask and (A) the antisaccade map (z coordinate = 49); (B) the mental rotation map (z coordinate = 49); and (C) the task conjunction map. (D) A surface rendered view with inset highlighting alignment of the IPS task conjunction map along the right IPS. Blue regions indicate the IPS mask, purple regions indicate the overlap between the IPS mask and the task conjunction map, and the red regions indicate activity outside of the IPS mask. Activation maps thresholded at $P_{FDR} < 0.05$, $k > 25$. Abbreviation: IPS, intraparietal sulcus. [Color figure can be viewed at wileyonlinelibrary.com]

anteriorly to posteriorly along the medial bank of the IPS, and predominantly in the right hemisphere.

The majority of the activated voxels in the conjunction analysis were assigned bilaterally to cytoarchitectonically defined IPS subregion hIP3 (Fig. 5 and Table I). In the right hemisphere, 50.0% of the activated voxels were assigned to hIP3 (with relative extent of activation 30.1%) and 20.1% of activated voxels were assigned to hIP2 (with

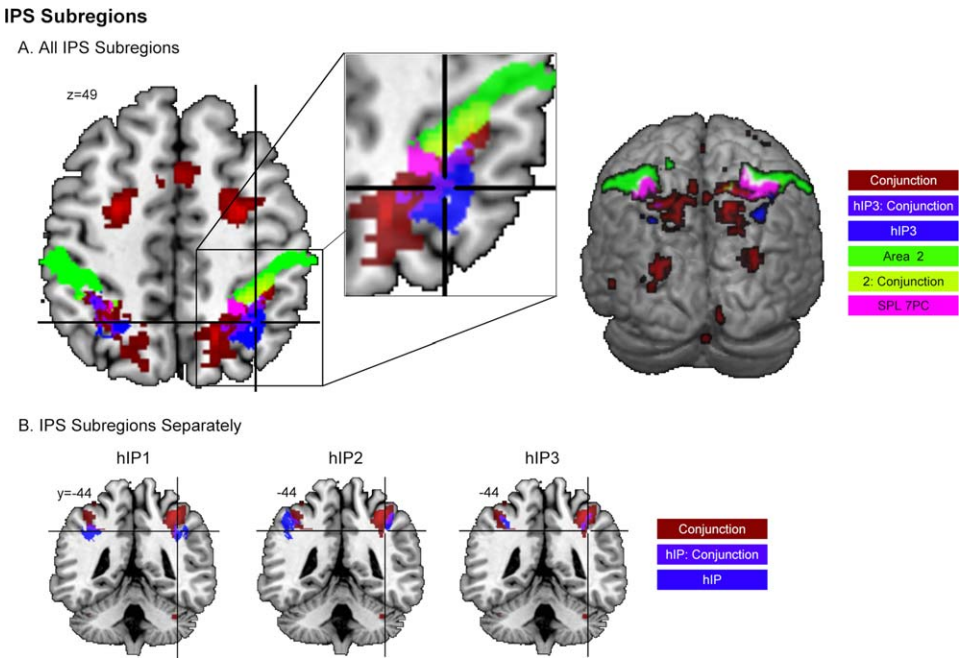

Figure 5.

IPS task conjunction of tasks within anatomical subregions of the parietal cortex. (a) All parietal subregions (z coordinate = 49), with detail shown along the IPS (inset) and across the posterior cortical surface (rendered view). (B) IPS subregion task conjunction maps for hIP1, hIP2, and hIP3 (y coordinate = −44). Blue regions indicate the IPS subregion masks, red regions indicate the significant conjunction between the mental rotation and antisaccade tasks, purple regions indicate the overlap of each IPS subregion map with the task conjunction map, green regions indicate the Area 2 anatomical mask, yellow regions indicate the overlap of the task conjunction map with the Area 2 mask, and pink regions indicate the SPL anatomical mask. Abbreviations: IPS, intraparietal sulcus; SPL, superior parietal lobule. [Color figure can be viewed at wileyonlinelibrary.com]

TABLE I. MNI coordinates, *T* values, and cluster sizes of regions showing statistical conjunction of antisaccade and mental rotation tasks

Percentage probabilities of cytoarchitectonic regions	Number of voxels in cluster	Site of SPM maxima *x*, *y*, *z* MNI coordinates	*T* value
R inferior parietal lobule/R superior parietal lobule/R angular gyrus	185		
(50.0%) hIP3 (30.1%)		40 −40 48	6.41
(20.1%) hIP2 (28.8%)		36 −46 54	5.67
(8.9%) hIP1 (7.2%)		38 −44 52	5.46
(6.1%) Area 2 (1.2%)		42 −40 52	5.36
(5.5%) SPL 7PC (2.5%)		32 −44 44	4.72
(3.0%) SPL 7A (0.5%)		26 −58 52	4.70
(0.6%) IPC PFt (0.3%)		36 −42 44	4.66
(0.1%) IPC PFm (0.0%)		22 −56 50	4.57
		32 −52 54	4.14
		26 −62 46	3.85
		30 −56 46	3.81
L inferior parietal lobule/L postcentral gyrus/L superior parietal lobule	105		
(59.4%) hIP3 (22.3%)		−30 −52 48	5.05
(17.7%) hIP1 (4.1%)		−32 −48 50	4.39
(6.7%) hIP2 (3.1%)		−40 −36 42	4.28
(6.3%) SPL 7PC (3.3%)		−40 −44 48	4.10
(3.2%) Area 2 (0.4%)		−26 −58 54	3.78
(1.1%) SPL 7A (0.1%)		−28 −46 42	3.64
(0.5%) IPC PFt (0.1%)		−34 −42 40	3.57
(0.4%) SPL 5L (0.1%)		−36 −46 54	3.56
(0.1%) Area 1 (0.0%)		−28 −60 44	3.38
L superior parietal lobule	1		
(75.0%) hIP3 (0.3%)		−22 −56 52	3.26
(25.0%) SPL 7A (0.0%)			

The anatomical region and cytoarchitectonic map location [Eickhoff et al., 2005] of significant clusters ($P < 0.05$ corrected) for the conjunction of antisaccade and mental rotation tasks at the group level. Percentage probabilities for cytoarchitectonic locations are based on the maximum probability map, version 1.3 [Eickhoff et al., 2005]; for example, "50.0% hIP3 (30.1%)" indicates that 50.0% of the cluster activation is in hIP3 and this represents 30.1% activation of the total volume for hIP3. Cluster size is based on number of voxels at $P < 0.05$ FDR corrected within cluster. Site of maxima voxels (Montreal Neurological Institute (MNI) *x*, *y*, *z* coordinates) and peak voxel *Z* scores reported also reached significance at a false discovery rate (FDR) probability threshold $P < 0.05$. Area 1 = Brodman Area 1; Area 2 = Brodman Area 2; hIP1 = human intraparietal area 1; hIP2 = human intraparietal area 2; hIP3 = human intraparietal area 3; IPC = inferior parietal cortex; SPL = superior parietal lobule.

relative extent of activation 28.8%). Small percentages of this cluster were identified as being in hIP1 (8.9%), Brodmann Area 2 (BA2; 6.1%) and the superior parietal lobule 7PC (SPL 7PC; 5.5%). In the left hemisphere, 59.4% of activated voxels were assigned to hIP3 (with relative extent of activation 22.3%), and 17.7% of activated voxels were assigned to hIP1 (with relative extent of activation 4.1%). Small percentages of this cluster were identified as hIP2 (6.7%), SPL 7PC (6.3%), Brodmann Area 2 (BA2; 3.2%), and SPL 7A (1.1%).

Figure 6 shows the consistency of results across individuals. These maps highlight that the antisaccade task cluster within the IPS was the most consistent across individuals, with all 14 participants contributing to the peak. The mental rotation task cluster within the IPS had 10 individuals contribute to the peak, and 8 individuals contributed to the IPS peak in the conjunction of the antisaccade and mental rotation tasks.

The sample size of this study is modest, and the sample included demographic variance in age, sex and handedness, which were not controlled for in the main analysis. Therefore, we conducted follow-up permutation tests to examine the reproducibility of the results. After controlling for age, sex and handedness, the conjunction results were largely consistent with the main analysis (Table II). In the right hemisphere, the IPS cluster increased from 185 voxels in the main analysis, to 193 voxels after controlling for age, sex, and handedness. The percentage of activation remained largely within hIP3 (from 50% to 63%); the percentage of activation within hIP2 reduced (from 20% to 3%) and hIP1 remained largely unchanged (from 9% to 7%). In the left hemisphere, the IPS cluster size remained unchanged. The percentage of activation within hIP3 and hIP2 reduced after controlling for demographic variance (hIP3: from 60% to 40%; hIP2: from 7% to 0.4%); the

TABLE II. MNI coordinates and cluster sizes of regions showing statistical conjunction of antisaccade and mental rotation tasks in permutation tests: controlling for age, sex, and handedness

	Nonparametric tests		Values in main analysis	
Probabilistic mapping	# Voxels	Maxima	# Voxels	Probabilities
R inferior parietal lobule/R superior parietal lobule/R angular gyrus	193	36 −44 48	185	
(62.9%) hIP3 (26.5%)				(50.0%) hIP3 (30.1%)
(7.3%) hIP1 (4.9%)				(8.9%) hIP1 (7.2%)
(3.4%) hIP2 (3.1%)				(20.1%) hIP2 (28.8%)
(1.9%) Area 2 (0.6%)				(6.1%) Area 2 (1.2%)
(0.8%) SPL 7A (0.2%)				(3.0%) SPL 7A (0.5%)
(0.7%) SPL 7PC (0.3%)				(5.5%) SPL 7PC (2.5%)
				(0.6%) IPC PFt (0.3%)
				(0.1%) IPC PFm (0.0%)
L inferior parietal lobule/L postcentral gyrus/L superior parietal lobule	105	−36 −52 50	105	
(39.8%) hIP3 (9.1%)				(59.4%) hIP3 (22.3%)
(33.3%) hIP1 (9.6%)				(17.7%) hIP1 (4.1%)
(0.4%) hIP2 (0.2%)				(6.7%) hIP2 (3.1%)
(2.7%) Area 2 (0.5%)				(3.2%) Area 2 (0.4%)
(1.7%) IPC PFt (0.3%)				(0.5%) IPC PFt (0.1%)
(0.2%) SPL 5L (0.1%)				(0.4%) SPL 5L (0.1%)
				(6.3%) SPL 7PC (3.3%)
				(1.1%) SPL 7A (0.1%)
				(0.1%) Area 1 (0.0%)
L superior parietal lobule	7	−28 −60 46	1	
(89.3%) hIP3 (1.4%)				(75.0%) hIP3 (0.3%)
				(25.0%) SPL 7A (0.0%)

Values from the main analysis (see main text) are shown for ease of comparison. The anatomical region and cytoarchitectonic map location [Eickhoff et al., 2005] of significant clusters ($P < 0.05$ corrected) for the conjunction of antisaccade and mental rotation tasks at the group level. Percentage probabilities for cytoarchitectonic locations are based on the maximum probability map, version 1.3 [Eickhoff et al., 2005]; for example, "50.0% hIP3 (30.1%)" indicates that 50.0% of the cluster activation is in hIP3 and this represents 30.1% activation of the total volume for hIP3. Cluster size is based on number of voxels at $P < 0.05$ FDR corrected within cluster. Site of maxima voxels (Montreal Neurological Institute (MNI) x, y, z coordinates) and peak voxel Z scores reported also reached significance at a false discovery rate (FDR) probability threshold $P < 0.05$. Area 1 = Brodman Area 1; Area 2 = Brodman Area 2; hIP1 = human intraparietal area 1; hIP2 = human intraparietal area 2; hIP3 = human intraparietal area 3; IPC = inferior parietal cortex; SPL = superior parietal lobule.

percentage of activation within hIP1 increased (from 18% to 33%) after controlling for demographic variables. Last, the third cluster in the left hIP3 increased slightly in size (from 1 to 7 voxels). These results confirm that the conjunction is robust when controlling for sample age, sex, and handedness.

Figure 7 shows the results of the classification analysis. The GNB classifier achieved a high accuracy in hIP1 (85.7%) and hIP2 (82.1%), suggesting that the activity patterns within these two IPS subregions was spatially distinct. A lower accuracy was achieved in hIP3 (64.3%), suggesting that the spatial pattern of the activity for the tasks was similar in this subregion. Dice coefficients further corroborated those findings. The DCS between the binarized accuracy map (1 where classification accuracy > 50%) and hIP1 was 0.51, confirming that the area with the highest classification accuracy has a significant spatial overlap with the ROI representing hIP1 subregion. Following the decreasing trend observed for the GNB classifier accuracy, the DCS for hIP2 and hIP3 were 0.26 and 0.15, respectively. In particular, the low DCS for hIP3, denoting a small number of voxels with high classification accuracy in this area, is a further evidence of the inability of the classifier to distinguish between the two tasks in this subregion (Fig. 7).

DISCUSSION

The goal of this preliminary study was to determine if object-based visuospatial transformation is a unitary process that is invoked regardless of current context, behavioral goals, and current task rules. Drawing upon previous studies, we argued that object-based visuospatial transformation is localized to the intraparietal sulcus. We used the antisaccade and mental rotation tasks, two tasks that

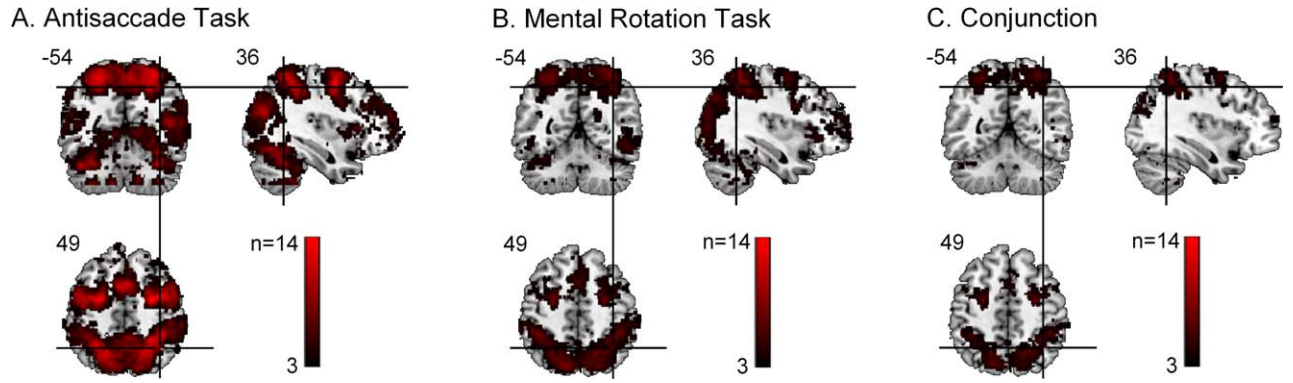

Figure 6.

Consistency of results. (a) Antisaccade task had all 14 participants contribute to the peak of activity within the IPS cluster. (b) The mental rotation task had 71% (10/14) participants contribute to the peak of activity within the IPS. (c) The conjunction between antisaccade and mental rotation maps had 57% (8/14) participants contribute to the peak of activity within the IPS. [Color figure can be viewed at wileyonlinelibrary.com]

require visuospatial transformation, and that show robust activation of the IPS. The results obtained from whole-brain analyses for each task were consistent with the literature demonstrating activation of medial and posterior IPS during the antisaccade task [Domagalik et al., 2012; Jamadar et al., 2013, 2015] and the medial, ventral, and posterior medial IPS during the mental rotation task [Podzebenko et al., 2002, 2005; Weiss et al., 2009]. These results are consistent with evidence showing that neurons within the human IPS code for visuospatial transformation [Choi et al., 2006; Grefkes and Fink, 2005].

We tested the hypothesis that the IPS is involved in object-based visuospatial transformation in a non-context-dependent manner by using three approaches: (a) statistical conjunction analysis testing for co-activation of the IPS in the antisaccade and mental rotation tasks; (b) statistical parametric anatomical mapping to localize activity to IPS subregions; and (c) a Gaussian naïve Bayes (GNB) classifier to test if activity of IPS subregions can be discriminated between tasks. To examine the reproducibility of the IPS results, consistency analyses and nonparametric tests controlling for demographic variance in age, sex, and handedness were also conducted.

The majority (50%) of the significant statistical conjunction was obtained between the two tasks in the medial and posterior medial aspects of the IPS, particularly area hIP3. Permutation tests confirmed that this result was not due to variance in age, sex, and handedness. While a statistically significant conjunction provides evidence of co-activation of the same region between tasks, this analysis does not confirm that the activity is identical between the two tasks. The GNB classifier demonstrated poor classification accuracy in area hIP3, confirming that the activity within this region was indiscriminable between the two tasks. This result is strong evidence that this region performs a "general purpose," non-context-dependent role in object-based visuospatial transformation, compatible with this region's involvement in the multidemand network [Duncan, 2010]. In contrast, while 20% of the conjunction between antisaccade and mental rotation tasks was

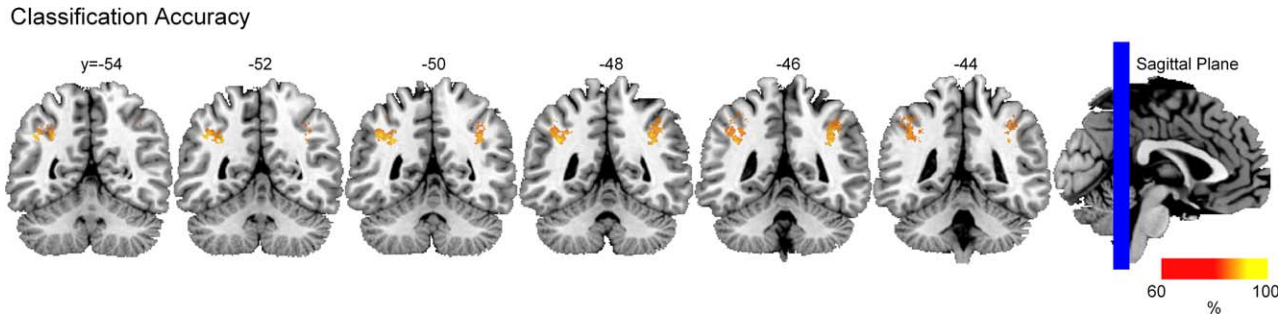

Figure 7.

Classification accuracy. Highlighted areas indicate the percent accuracy for the classification analysis. [Color figure can be viewed at wileyonlinelibrary.com]

obtained in hIP2, the GNB classifier showed very high classification accuracy (82%) between the two tasks in this region. While only a small proportion (<10%) of the significant conjunction between the tasks was obtained in hIP1, this region showed the highest classification accuracy (86%) between the tasks. These results represent an interesting dissociation between these three regions and their involvement in visuospatial transformation. Region hIP2 appears to be significantly activated by visuo-spatial transformation, but appears to play a distinct role in each task. Region hIP1 is minimally activated by visuospatial transformation, and is likely to play a different role in antisaccade and mental rotation. In contrast, region hIP3 is involved in a visuospatial transformation that is common and indistinguishable between the two tasks.

The functional and structural connectivity and cytoarchitectonic profile of region hIP3 is different from regions hIP1 and hIP2. The cytoarchitectonic laminar pattern of region hIP3 shows significantly different border patterns between layers and different volume of cell bodies compared to the neighboring regions [Scheperjans et al. 2008b]. Region hIP3 shows greater functional connectivity to visual cortex and greater density of fibers along the inferior fronto-occipital fasciculus connecting to the superior occipital cortex, compared to regions hIP1 and hIP2, which show greater functional and structural connectivity to fronto-parietal networks [Uddin et al., 2010]. Thus our results are compatible with previous studies showing that region hIP3 shows a distinct anatomical and functional profile compared to regions hIP1 and hIP2. The greater structural and functional connectivity of hIP3 to visual cortex underscores its role in manipulating visual information for subsequent processing. Although region hIP3 has only recently been identified in cytoarchitectonic maps of the IPS [Scheperjans et al., 2008a, 2008b], evidence is building that this region plays a critical role in visuospatial attention. Gillebert et al. [2013] concluded that this region is involved in attentional selection between peripherally presented stimuli. Silk et al. [2010] concluded that hIP3 maintains a spatial map where coordinates of an attention shift are computed based on motor planning (see also Corbetta et al. [2002] and Hu et al. [2009]); consistent with the vector inversion process in the antisaccade task [Medendorp et al., 2005] and isomorphic nature of mental rotation [Zacks and Michelon, 2005].

In contrast, the greater connectivity of region hIP2 with fronto-parietal networks for action, suggests that this region may be important for transforming the visuospatial information into a target for action. While the antisaccade and mental rotation tasks share common processes including target identification and visuospatial transformation, the two tasks differ in the processing that occurs after transformation. In the antisaccade task, the result of the transformation process directly codes the location for the eye movement, and the saccade is performed. In the mental rotation task, the result of the transformation process must be parsed to category-response rules (i.e., correct orientation = left hand; mirror orientation = right hand), and the result of that decision process is then parsed to the motor output. We argue that region hIP2 plays an important role in converting the result of the visuospatial transformation carried out by hIP3 into a target for action.

Importantly, we do not claim that the IPS subdivisions *only* perform visuo-spatial transformation (hIP3), or *only* visuo-motor integration (hIP2); rather we argue that the present results support the conclusion that visuospatial transformation is a unitary process that is common across tasks and is implemented by a distinct region of the IPS. Interestingly, this serial view of visuospatial transformation in hIP3 and visuomotor integration in hIP2 is consistent with the known temporal properties of the IPS during antisaccades. Nyffeler et al. [2008] showed that the initial process of vector inversion during antisaccades can be disrupted using transcranial magnetic stimulation (TMS) early (100 ms) after the onset of the target. TMS applied later (330–450 ms) after target onset interfered with integrating the result of the vector inversion with motor saccade planning. These results are consistent with our argument that the visuospatial transformation performed by hIP3 is parsed to hIP2 for integration with motor action plans. This serial view is also consistent with arguments that the IPS is part of a domain-general multidemand network that is recruited across a broad range of tasks [Duncan, 2010; Fedorenko et al., 2013].

Our results are compatible with the characterization of the posterior parietal cortex as a multimodal association region, which processes different input modalities for integration into higher cognitive, motor, and somatosensory processing. The IPS in particular has long been recognized as playing an important role in integrating visual information with spatial, motor, and somatosensory information to support successful hand-eye coordination and movement through the environment [Grefkes et al., 2004; Corbetta et al., 2002; Colby and Goldberg, 1999]. Our results are also compatible with the apparent modular organization of the IPS, evident from architectonic, electrophysiological, and functional studies of the macaque and human (reviewed in Caspers et al. [2012]). Thus, the IPS appears to be composed of a number of highly specialized modules that play a general role in visual attention that are selectively activated during a variety of cognitive processes, and are integrated into complex fronto-parietal and parieto-occipital networks that subserve goal-directed and object-centered movements [Grefkes et al., 2004].

Given that cognitive neuroscience appears to be building evidence against the concept of modularity in human brain function (see, e.g., discussions in Hanson and Bunzl [2010]), the question arises, why would there be regions within the parietal cortex specialized for object-based visuospatial transformation? The integrative processes mediated by the IPS, including visuospatial transformation, are vital for the successful interaction of the organism

with the external environment. Interacting with the world requires anticipating the consequences of one's own actions, as well as the actions of other people and objects in the environment. IPS-mediated visuospatial transformation underlies the human ability for exquisitely fine hand–eye coordination [Grefkes et al., 2004], highly detailed and person-centric action observation and monitoring [Caspers et al., 2010], powerful allocation of attention to location [Fink et al., 1997], and the ability to transform symbolic information to spatial and semantic representations of quantity and semantic concepts [Dehaene et al., 2004; Uddin et al., 2010]. In turn, this allows the organism to use the present state to predict future outcomes (e.g., "Does this lid fit this plastic container?" "Can the lion fit through the gap to eat me?"), by imagining and transforming the visuospatial information present in the environment.

An interesting consequence of our findings is that if a single region mediates visuospatial transformation across tasks, it is likely that it is not possible to perform both antisaccade and mental rotation tasks simultaneously. It is a central tenet of classic cognitive psychology that a processing module that is in use by one task cannot be simultaneously used by another task. Irwin and Brockmole [2000] concluded that mental rotation is delayed until saccade processing is complete. Nyffeler et al. [2007] described a patient with a lesion in the right posterior parietal cortex resulting from an ischemic stroke. While visually guided saccades were intact, the patient was unable to perform antisaccades in the ipsilateral visual hemifield, nor was he able to perform mental rotation. This result is consistent with a modular view of object-based visuospatial transformation localized to the posterior parietal cortex.

Our results are also consistent with formulations of the "multiple demand" network [Duncan, 2010]: a common fronto-parietal network associated with diverse cognitive processes. In this model, goals are achieved in a strictly serial fashion, assembling a series of subtasks, each separately defined and solved. Broadly compatible with our results, Fedorenko et al. [2013] showed that an inferior parietal region that encompassed parts of the IPS showed a domain-general response across multiple tasks. Considered in light of this model, our results suggest that the IPS is specifically involved in an object-based visuospatial transformation subtask that is invoked for any global goal that requires such visuospatial transformation.

The study had a number of limitations, which should be considered in the development of future studies. One limitation is that we focused on a group-level rather than individual-level analysis. The IPS shows considerable interindividual variability in length and morphology [Choi et al., 2006; Scheperjans et al., 2008a, 2008b]; future studies should consider interindividual variability in IPS morphometry. Similarly, we did not control for differences in handedness or sex in our sample, which is known to influence cerebral morphology and asymmetry of brain structures [Good et al., 2001]. To control for these variables, we conducted non-parametric tests of the conjunction in the IPS, controlling for age, sex, and handedness. These results were consistent with the parametric tests, suggesting the current results are not driven by sample characteristics. Furthermore, we partly addressed each of these issues by using probabilistic anatomical mapping, and examining the consistency of our results across subjects, which confirmed that the majority of subjects contributed to the peak of activity in both tasks. One way to improve the examination of interindividual variability is to take the approach used by Fedorenko et al. [2013], who used subject-specific ROIs to study the consistency of activation across tasks. Connectivity analyses (e.g., psychophysiological interactions) should also consider the inter-relatedness of activity between brain regions during object-based visuospatial transformation. It may also be possible in the future to use a combination of structural imaging (e.g., diffusion tensor imaging) together with functional imaging to map region hIP3 and its role in object-based visuospatial transformation.

In conclusion, the results of this study suggest that object-based visuospatial transformation is a unitary domain-general process that is localized to the IPS, specifically, the hIP3 subdivision. Our results are consistent with the modular model of the posterior parietal cortex and the distinct cytoarchitectonic, structural, and functional connectivity profiles of the subregions in the intraparietal sulcus.

AUTHOR CONTRIBUTIONS

Conceptualization and methodology: SJ and GE. Formal analysis: AP and FS. Writing, original draft: AP, FS and SJ. Writing, review and editing: SJ and GE.

ACKNOWLEDGMENTS

The authors thank Mr Richard McIntyre for assistance with data acquisition, Dr Beth Johnson for training on oculomotor analyses, and Assoc Prof Joanne Fielding for comments on previous versions of this article.

The authors declare no conflicts of interest.

REFERENCES

Alivisatos B, Petrides M (1997): Functional activation of the human brain during mental rotation. Neuropsychologia 35: 111–118.

Booth JR, MacWhinney B, Thulborn KR, Sacco K, Voyvodic JT, Feldman HM (2000): Developmental and lesion effects in brain activation during sentence comprehension and mental rotation. Dev Neuropsychol 18:139–169.

Brown MRG, Goltz HC, Vilis T, Ford KA, Everling S (2006): Inhibition and generation of saccades: Rapid event-related fMRI of prosaccades, antisaccades, and nogo trials. NeuroImage 33: 644–659.

Caspers S, Amunts K, Zilles K (2012): Posterior parietal cortex: Multimodal association cortex. In Mai JK, Paxinos G, editors.

The Human Nervous System, 3rd ed. Boston: Elsevier Academic Press. pp. 1036–1055.
Caspers S, Eickhoff SB, Geyer S, Scheperjans F, Mohlberg H, Zilles K, Amunts K (2008): The human inferior parietal lobule in stereotaxic space. Brain Struct Funct 212:481–495.
Caspers S, Zilles K, Laird AR, Eickhoff SB (2010): ALE meta-analysis of action observation and imitation in the human brain. NeuroImage 50:1148–1167.
Choi HJ, Zilles K, Mohlberg H, Schleicher A, Fink GR, Armstrong E, Amunts K (2006): Cytoarchitectonic identification and probabilistic mapping of two distinct areas within the anterior ventral bank of the human intraparietal sulcus. J Comparat Neurol 495:53–69.
Cohen MS, Kosslyn SM, Breiter HC, DiGirolamo GJ, Thompson WL, Anderson AK, ... Belliveau JW (1996): Changes in cortical activity during mental rotation: A mapping study using functional MRI. Brain 119:89–100.
Colby CL, Goldberg ME (1999): Space and attention in parietal cortex. Annu Rev Neurosci 22:319–349.
Corbetta M, Kincade JM, Shulman GL (2002): Neural systems for visual orienting and their relationships to spatial working memory. J Cogn Neurosci 14:508–523.
Culham JC, Valyear KF (2006): Human parietal cortex in action. Curr Opin Neurbiol 16:205–212.
Dehaene S, Molko N, Cohen L, Wilson AJ (2004): Arithmetic and the brain. Curr Opin Neurbiol 14:218–224.
Domagalik A, Beldzik E, Fafrowicz M, Oginska H, Marek T (2012): Neural networks related to pro-saccades and anti-saccades revealed by independent component analysis. NeuroImage 62:1325–1333.
Duncan J (2010): The multiple-demand system of the primate brain: Mental programs for intelligent behaviour. Trends Cogn Sci 14:172–179.
Dyckman KA, Camchong J, Clementz BA, McDowell JE (2007): An effect of context on saccade-related behavior and brain activity. NeuroImage 36:774–784.
Eickhoff SB, Heim S, Zilles K, Amunts K (2006): Testing anatomically specified hypotheses in functional imaging using cytoarchitectonic maps. NeuroImage 32:570–582.
Eickhoff SB, Stephan KE, Mohlberg H, Grefkes C, Fink GR, Amunts K, Zilles K (2005): A new SPM toolbox for combining probabilistic cytoarchitectonic maps and functional imaging data. NeuroImage 25:1325–1335.
Enderle JD (2010): Part I: Early models of saccades and smooth pursuit models of horizontal eye movements. In Enderle JD, Series editor. Synthesis Lectures on Biomedical Engineering. Morgan & Claypool Publishers.
Fedorenko E, Duncan J, Kanwisher N (2013): Broad domain generality in focal regions of frontal and parietal cortex. Proc Natl Acad Sci 110:16616–16621.
Fink GR, Dolan RJ, Halligan PW, Marshall JC, Frith CD (1997): Space-based and object-based visual attention: Shared and specific neural domains. Brain 120:2013–2028.
Gillebert CR, Mantini D, Peeters R, Dupont P, Vandenberghe R (2013): Cytoarchitectonic mapping of attentional selection and reorienting in parietal cortex. NeuroImage 67:257–272.
Goebel R, Linden DE, Lanfermann H, Zanella FE, Singer W (1998): Functional imaging of mirror and inverse reading reveals separate coactivated networks for oculomotion and spatial transformations. NeuroReport 9:713–719.
Gogos A, Gavrilescu M, Davison S, Searle K, Adams J, Rossell SL, ... Egan GF (2010): Greater superior than inferior parietal lobule activation with increasing rotation angle during mental rotation: An fMRI study. Neuropsychologia 48:529–535.
Good CD, Johnsrude I, Ashburner J, Henson RNA, Friston KJ, Frackowiak RSJ (2001): Cerebral asymmetry and the effects of ex and handedness on brain structure: A voxel-based morphometric analysis of 465 normal adult human brains. NeuroImage 14: 685–700.
Grefkes C, Fink GR (2005): The functional organisation of the intraparietal sulcus in humans and monkeys. J Anat 207:3–17.
Grefkes C, Ritzl A, Zilles K, Fink GR (2004): Human medial intraparietal cortex subserves visuomotor coordinate transformation. NeuroImage 23:1494–1506.
Hanson SJ, Bunzl M (2010): Foundational Issues in Human Brain Mapping. MIT Press.
Hebart MN, Görgen K, Haynes JD (2015): The Decoding Toolbox (TDT): A versatile software package for multivariate analyses of functional imaging data. Front Neuroinformatics 8: doi: 10.3389/fninf.2014.00088.
Hoffstaedter F, Grefkes C, Caspers S, Roski C, Palomero-Gallagher N, Laird AR, ... Eickhoff SB (2013): The role of anterior midcingulate cortex in cognitive motor control: Evidence from functional connectivity analyses. Hum Brain Mapp. doi: 10.1002/hbm.22363
Hu S, Bu Y, Song Y, Zhen Z, Liu J (2009): Dissociation of attention and intention in human posterior parietal cortex: An fMRI study. Eur J Neurosci 29:2083–2091.
Irwin DE, Brockmole JR (2000): Mental rotation is suppressed during saccadic eye movements. Psychonom Bull Rev 7:654–661.
Jamadar SD, Fielding J, Egan G (2013): Quantitative meta-analysis reveals consistent fMRI activation in fronto-striatal- parietal regions and cerebellum during antisaccades and prosaccades. Front Psychol. doi: 10.3389/fpsyg.2013.00749
Jamadar SD, Johnson BP, Clough M, Egan GF, Fielding J (2015): Behavioral and neural plasticity of ocular motor control: Changes in performance and fMRI activity following antisaccade training. Front Hum Neurosci 9. doi: 10.3389/fnhum.2015.00653.
Koyama M, Hasegawa I, Osada T, Adachi Y, Nakahara K, Miyashita Y (2004): Functional magnetic resonance imaging of macaque monkeys performing visually guided saccade tasks: Comparison of cortical eye fields with humans. Neuron 41:795–807.
McDowell JE, Dyckman KA, Austin BP, Clementz BA (2008): Neurophysiology and neuroanatomy of reflexive and volitional saccades: Evidence from studies of humans. Brain Cogn 68: 255–270.
Medendorp WP, Goltz HC, Vilis T (2005): Remapping the remembered target location for antisaccades in human posterior parietal cortex. J Neurophysiol 94:734–740.
Milivojevic B, Hamm JP, Corballis MC (2009): Functional neuroanatomy of mental rotation. J Cogn Neurosci 21:945–959.
Mitchell DJ, Bell AH, Buckley MJ, Mitchell AS, Sallet J, Duncan J (2016): A putative multiple-demand system in the macaque brain. Journal of Neuroscience 36:8574–8585.
Moon SY, Barton JJS, Mikulski S, Polli FE, Cain MS, Vangel M, ... Manoach DS (2007): Where left becomes right: A magnetoencephalographic study of sensorimotor transformation for antisaccades. NeuroImage 36:1313–1323.
Munoz DP, Everling S (2004): Look away: The anti-saccade task and the voluntary control of eye movement. Nat Rev Neurosci 5:218–228.
Nyffeler T, Rivaud-Pechoux S, Pierrot-Deseilligny C, Diallo R, Gaymard B (2007): Visual vector inversion in the posterior parietal cortex. NeuroReport 18:917–920.

Nyffeler T, Hartmann M, Hess CW, Müri RM (2008): Visual vector inversion during memory antisaccades—a TMS study. Progr Brain Res 171:429–432.

Oldfield RC (1971): The assessment and analysis of handedness: The Edinburgh inventory. Neuropsychologia 9:97–113.

Pierrot-Deseilligny C, Milea D, Muri RM (2004): Eye movement control by the cerebral cortex. Curr Opin Neurbiol 17:17–25.

Podzebenko K, Egan GF, Watson JD (2002): Widespread dorsal stream activation during a parametric mental rotation task, revealed with functional magnetic resonance imaging. NeuroImage 15:547–558.

Podzebenko K, Egan GF, Watson JDG (2005): Real and imaginary rotary motion processing: Functional parcellation of the human parietal lobe revealed by fMRI. J Cogn Neurosci 17:24–36.

Schendan HE, Stern CE (2007): Mental rotation and object categorization share a common network of prefrontal and dorsal and ventral regions of posterior cortex. NeuroImage 35:1264–1277.

Scheperjans F, Eickhoff SB, Hömke L, Mohlberg H, Hermann K, Amunts K, Zilles K (2008a): Probabilistic maps, morphometry, and variability of cytoarchitectonic areas in the human superior parietal cortex. Cereb Cortex 18:2141–2157.

Scheperjans F, Hermann K, Eickhoff SB, Amunts K, Schleicher A, Zilles K (2008b): Observer-independent cytoarchitectonic mapping of the human superior parietal cortex. Cereb Cortex 18: 846–867.

Sereno MI, Pitzalis S, Martinez A (2001): Mapping of contralateral space in retinotopic coordinates by a parietal cortical area in humans. Science 294:1350–1354.

Silk TJ, Bellgrove MA, Wrafter P, Mattingley JB, Cunnington R (2010): Spatial working memory and spatial attention rely on common neural processes in the intraparietal sulcus. NeuroImage 53:718–724.

Uddin LQ, Supekar K, Amin H, Rykhlevskaia E, Nguyen DA, Greicius MD, Menon V (2010): Dissociable connectivity within human angular gyrus and intraparietal sulcus: Evidence from functional and structural connectivity. Cereb Cortex 20: 2636–2646.

Vandenberghe R, Gillebert CR (2009): Parcellation of parietal cortex: Convergence between lesion-symptom mapping and mapping of the intact functioning brain. Behav Brain Res 199:171–182.

Weiss MM, Wolbers T, Peller M, Witt K, Marshall L, Buchel C, Siebner HR (2009): Rotated alphanumeric characters do not automatically activate frontoparietal areas subserving mental rotation. NeuroImage 44:1063–1073.

Wilke M (2012): An alternative approach towards assessing and accounting for individual motion in fMRI timeseries. NeuroImage 59:2062–2072.

Wilke M (2014): Isolated assessment of translation or rotation severely underestimates the effects of subject motion in fMRI data. PLoS One. doi: 10.1371/journal.pone.0106498.

Wu SS, Chang TT, Majid A, Caspers S, Eickhoff SB, Menon V (2009): Functional heterogeneity of inferior parietal cortex during mathematical cognition assessed with cytoarchitectonic probability maps. Cereb Cortex 19:2930–2945.

Zacks JM (2008): Neuroimaging studies of mental rotation: A meta-analysis and review. J Cogn Neurosci 20:1–19.

Zacks JM, Michelon P (2005): Transformations of visuospatial images. Behav Cogn Neurosci Rev 4:96–118.

Zhang M, Barash S (2000): Neuronal switching of sensorimotor transformations for antisaccades. Nature 408:971–975.